Tidal Heating via Internal Gravity Waves in White Dwarf Binaries

Authors

(Dated: February 25, 2019)

In white dwarf binaries tidal torques are expected to raise a train of internal gravity waves in the white dwarf interior. These outward-propagating waves can then grow to be nonlinear and break via hydrodynamical instabilities, transfering energy and angular momentum from the binary orbit to the white dwarf. We perform 2D numerical simulations of nonlinear wave breaking of outwards-propagating internal gravity waves in an incompressible, isothermal atmosphere with an exponentially decaying density stratification. We find that tidal synchronization, after an initial transient phase, proceeds inwards from the surface in thin layers. We argue the thickness of these layers is limited by the Kelvin-Helmholtz Instability. We provide simple analytical formulae for the location and thickness of tidal synchronization over time that are in good agreement with our simulations.

I. INTRODUCTION

Compact white dwarf (WD) binary systems, with orbital periods in the range of minutes to hours, are important for a range of astrophysical problems. They are the most important sources of gravitational waves (GWs) for the Laser Interferometric Space Antenna (LISA)[1]. They are also thought to produce interesting optical transients such as underluminous supernovae[2], Ca-rich fast transients[3], and tidal novae[4]. Most importantly, they have been proposed as the likely progenitors of type Ia supernovae (e.g. [5, 6] or more recently[7, 8]). While presently only a few tens of compact WD binaries are known[9], *Gaia* (currently gathering data) is expected to expand the catalog to a few hundreds[9] (results based on *Gaia*'s second data release have already begun to appear[10, 11]), and the Large Synoptic Survey Telescope (LSST, first light scheduled for 2020) will likely detect a few thousand more[9]. These observations will significantly advance the understanding of WD binaries and their evolution. My proposed theoretical and computational research is well-timed to take advantage of these new advances.

In spite of the broad importance of WD binaries, the evolution of these systems prior to their final mergers is not well understood. Much of this uncertainty comes from our imprecise understanding of tidal interactions, which play an important role during a compact WD binary's inspiral[12]. Previous studies have shown that these interactions manifest as tidal excitation of internal gravity waves (IGW), waves in the WD fluid restored by the buoyancy force due to density stratification[13]. As these waves propagate outwards towards the WD surface, they grow in amplitude until they break, as do ocean waves on a shore, and transfer both energy and angular momentum from the binary orbit to the outer envelope of the WD[12, 13].

Previous works have found that the dissipation of IGW can generate significantly more energy than thermal radiation from the isolated WD surface and is thus a major contributor to the WD energy budget[12, 14]. However, these works parameterized the wave breaking process in an ad hoc manner. The details of dissipation, namely the location and spatial extent of the wave breaking, affect the observable outcome: dissipation near the surface of the WD can be efficiently radiated away and simply brightens the WD, while dissipation deep in the WD envelope causes an energy buildup that results in energetic flares[4]. Works in other fields based on numerical simulations show that strongly nonlinear wave breaking behaves differently than predictions based in linear and weakly nonlinear theory[15, 16]. Such fully nonlinear numerical simulations have not been performed for WDs.

In §II, we will describe the system of equations we will use to analyze IGW breaking. In §III, we discuss relevant analytical results. In §IV we present the results of numerical simulations. Finally, in §V we discuss the results of the preceeding section.

II. PROBLEM DESCRIPTION

We consider an incompressible, isothermal fluid, representative of degenerate matter in WD bulks, in 2D. We neglect temperature variations and assume a barotropic equation of state as a first approximation. As we are interested in the behavior of the wave far from the center of the WD, we approximate the gravitational field as uniform. We model the background density stratification as $\rho_0(x,z) = \rho_0(z) = \rho_0(z=0)e^{-z/H}$ for some reference density $\rho_0(z=0) = \rho_0(z)|_{z=0}$.

The Euler equations for an incompressible, barotropic fluid in a uniform gravitational field are

$$\vec{\nabla}\cdot\vec{u} = 0, \tag{1a}$$

$$\frac{\mathrm{D}\rho}{\mathrm{D}t} = 0, \tag{1b}$$

$$\frac{\mathrm{D}\vec{u}}{\mathrm{D}t} + \frac{\vec{\nabla}p}{\rho} + g\hat{z} = 0.. \tag{1c}$$

$\frac{\mathrm{D}}{\mathrm{D}t} = \frac{\partial}{\partial t} + \left(\vec{u}\cdot\vec{\nabla}\right)$ is the Lagrangian or material derivative. $\vec{u}, \rho, p$ denote the velocity field, density and pressure respectively. We denote $-g\hat{z}$ constant gravitational acceleration. Note that at hydrostatic equilibrium $\frac{\partial}{\partial t} = 0$

we have $\vec{\nabla} P_0 = -\rho_0 g \hat{z}$ and so $P_0 = \rho_0 g H$. A shear flow $u_x(x,z,t) = u_x(z)$ is permitted in hydrostatic equilibrium, but we will initially consider no shear flow in equilibrium.

In practice, it is convenient to introduce coordinate $\Upsilon = \ln \frac{\rho}{\rho_0}$. This both identically enforces $\rho > 0$ and avoids numerical issues if ρ is small. We also define reduced pressure $P = \frac{p}{\rho}$. Then, we may rewrite the second two equations of Eq. 1 as

$$\frac{\mathrm{D}\Upsilon}{\mathrm{D}t} + u_z \frac{\partial \ln \rho_0}{\partial z} = 0, \tag{2a}$$

$$\frac{\mathrm{D}\vec{u}}{\mathrm{D}t} + \vec{\nabla} P + P \vec{\nabla} \Upsilon + g\hat{z} = 0. \tag{2b}$$

Note that in the new coordinates, hydrostatic equilibrium corresponds to $\Upsilon_0 = 1, P_0 = gH$.

III. INTERNAL GRAVITY WAVE THEORY

A. Analytical Properties: Linear

In the small perturbation limit, where flow velocities are small compared to the characteristic space and time scales $\frac{\partial}{\partial t} \gg \vec{u} \cdot \vec{\nabla}$, we may linearize Eq. 2. We ignore the advective components of the material derivative and consider small deviations $\Upsilon_1 = \Upsilon - \Upsilon_0, P_1 = P - P_0$ about hydrostatic equilibrium:

$$\vec{\nabla} \cdot \vec{u} = 0, \tag{3a}$$

$$\frac{\partial \Upsilon_1}{\partial t} - \frac{u_z}{H} = 0, \tag{3b}$$

$$\frac{\partial \vec{u}}{\partial t} + \vec{\nabla} P_1 + (1 + \Upsilon_1) g \hat{z} = 0. \tag{3c}$$

This can be solved to obtain solutions up to undetermined amplitude A the well-known result[17, 18]:

$$u_z(x,z,t) = A e^{z/2H} e^{i(k_{0x}x + k_{0z}z - \omega_0 t)}, \tag{4a}$$

$$\omega_0^2 = \frac{N^2 k_{0x}^2}{k_{0x}^2 + k_{0z}^2 + \frac{1}{4H^2}}, \tag{4b}$$

where

$$N^2 \equiv g^2 \left(\frac{\mathrm{d}\rho}{\mathrm{d}P} - \left.\frac{\partial \rho}{\partial P}\right|_{ad} \right) = \frac{g}{H}, \tag{5}$$

the Brunt-Väisälä frequency is constant

In the weak stratification limit $k_{0z} H \gg 1$, the solution exhibits the following characteristics:

- The amplitude of the perturbations grows like $e^{z/2H}$. Thus, the linear approximation is violated for sufficiently large z.

- The phase and group velocities can be computed respectively:

$$\vec{c}_{ph} = \left(\frac{\hat{x}}{k_{0x}} + \frac{\hat{z}}{k_{0z}} \right) \omega, \tag{6}$$

$$\vec{c}_g = \frac{N\left(k_{0x} k_{0z} \hat{x} - \left(k_{0z}^2 + \frac{1}{4H^2}\right)\hat{z}\right)}{\left(k_{0x}^2 + k_{0z}^2 + \frac{1}{4H^2}\right)^{3/2}} \approx \frac{\omega k_{0z}}{\left|\vec{k}_0\right|^{3/2}} (k_{0x}\hat{x} - k_{0z}\hat{z}). \tag{7}$$

  We recover the usual result $\vec{c}_{ph} \cdot \vec{c}_g = 0$ (e.g. [17, 19]). Note that an IGW transporting energy and momentum upwards $c_{g,z} > 0$ has $k_{0z} < 0$.

- The time-averaged total x-momentum flux in the $\hat{z}$ direction can be computed. Since the linear solution is separable as $f(x,z,t) = f(z) e^{i(k_{0x}x - \omega_0 t)}$, x averaging and time averaging are equivalent, so we may write

$$S_{px,z} \equiv \langle \rho u_x u_z \rangle_x \equiv \frac{1}{L_x} \int_0^{L_x} \rho u_x u_z \, \mathrm{d}x \approx -\frac{A^2}{2} \rho_0(z=0) \frac{k_{0z}}{k_{0x}}, \tag{8}$$

  where $\langle \ldots \rangle_x$ denotes x-averaging.

B. Wave Generation

To model a continuous IGW wave train excited deep in the WD interior propagating towards the surface, we use a volumetric forcing term to excite IGW near the bottom of the simulation domain[1]. Our forcing excites both IGWs propagating upwards, imitating a wave tidally excited deeper in the WD, and downwards, which are damped away by the damping layers described in §IV B.

As not to interfere with the incompressibility constraint, we force the system on the density equation. This constitutes replacing Eq. 2a with

$$\frac{\mathrm{D}\Upsilon}{\mathrm{D}t} + u_z \frac{\partial \ln \rho_0}{\partial z} = F e^{-\frac{(z-z_0)^2}{2\sigma^2}} \cos(k_{0x}x - \omega_0 t). \tag{9}$$

Using a narrow Gaussian profile excites a broad k_z wavenumber spectrum, and only the k_{0z} satisfying dispersion relation Eq. 4b for the given $k_{0x}, \omega_0(k_{0x}, k_{0z})$ will propagate.

In the linearized system, the effect of this forcing can be solved analytically up to good accuracy: we

[1] Interfacial forcing at the bottom boundary incurs strong stability limits, as we use a Chebyshev polynomial basis along the z axis in our spectral method which has very small grid spacing at the boundaries.

first approximate the driving term using $e^{\frac{-(z-z_0)^2}{2\sigma^2}} \approx \sqrt{2\pi\sigma^2}\delta(z-z_0)$, the $\sigma \to 0$ limit[2]. This system is solved exactly by matching the two homogeneous solutions above and below z_0. We may then approximately relax the solution to nonzero σ: an extra factor of $e^{-\frac{(k_{0z}\sigma)^2}{2}}$ arises compared to the δ-function solution (evaluating the Fourier Transform of $e^{-\frac{(z-z_0)^2}{2\sigma^2}}$ at $k_z = k_{0z}$), and we obtain

$$u_{1z}(x,z,t) = \frac{Fgk_{0x}^2}{\omega_0^2}\frac{1}{2ik_{0z}}\frac{e^{\frac{-(k_{0z}\sigma)^2}{2}}}{\sqrt{2\pi\sigma^2}}\times \begin{cases} e^{\frac{z-z_0}{2H}}e^{i\left(k_{0x}x+k_{0z}(z-z_0)-\omega_0 t+\frac{1}{2k_{0z}H}\right)} & z>z_0 \\ e^{\frac{z-z_0}{2H}}e^{i\left(k_{0x}x-k_{0z}(z-z_0)-\omega_0 t+\frac{1}{2k_{0z}H}\right)} & z<z_0 \end{cases}. \quad (10)$$

The $z > z_0$ solution models an upwards-propagating IGW wavetrain inbound on the simulation domain from below. The solution for $u_{1x}(x,z,t)$ is correspondingly $u_{1x} \approx \frac{k_{0z}u_{1z}}{k_{0x}}e^{\frac{i}{2k_{0z}H}}$.

C. Wave Breaking

In developing the results above, we have neglected advective terms $\frac{\partial}{\partial t} \gg \vec{u}\cdot\vec{\nabla}$. However, since $|\vec{u}| \propto e^{z/2H}$, any nonzero amplitude IGW will eventually violate the linearity criterion. This regime is relevant in practice since the IGW grows to nonlinear amplitudes before it reaches the surface of the WD[12, 13]. We can coarsely estimate the height at which this happens by $|\vec{u}|(z) \gtrsim \frac{\omega}{|\vec{k}|}$. This corresponds to when the Lagrangian displacement $\vec{\xi} \equiv \vec{u}/\omega$ satisfies $\vec{\xi}\cdot\vec{k} \gtrsim 1$, the same criterion used in[13].

The general understanding of nonlinear IGW breaking is that the waves' interactions with the mean flow of the fluid transfer horizontal momentum from the waves into the fluid; such a process has been conjectured to be responsible for tidal synchronization in stellar binaries[20, 21] as well as the quasi-biennial oscillation[22]. The details of this process have been laid out in a few key papers: IGWs are globally unstable to resonant three-wave interactions[17], causing energy transfer out of the IGW to daughter modes. These steeper daughter modes facilitate wave breaking, depositing horizontal momentum in the fluid's mean flow[23]. Once the mean flow reaches the horizontal phase velocity of the parent IGW, a critical layer forms at which the frequency of the IGW is Doppler-shifted to zero. The interaction of the parent IGW with the mean flow was first studied in the inviscid, linear regime in [24], which found nearly complete absorption. This result was reproduced with nonzero viscosity[25], but weakly nonlinear theory[26] and fully nonlinear simulations[15] suggest that nonlinear effects can induce reflection.

An estimate of where these mean flow effects become important can be made using the wave-induced mean flow formula[18, 27]:

$$\langle u_x\rangle = \bar{U}_0 \equiv \frac{1}{L_x}\int u_x \,\mathrm{d}x = \frac{\langle u_x u_z\rangle_x}{c_{g,z}}, \quad (11)$$

where $\langle\ldots\rangle x$ denotes horizontal averaging. Setting $\bar{U}_0 = c_{ph,x}$ the critical layer condition, we can solve that $\vec{\xi}\cdot\vec{k} = \sqrt{\frac{k_x}{k_z}}$ is where the mean flow attains the horizontal phase velocity. In an astrophysical context, $N \gg \omega$ and $k_z \gg k_x$. Thus, wave breaking may occur significantly earlier than assumed in current astrophysics literature.

IV. INTERNAL GRAVITY WAVE NUMERICAL SIMULATION

To study IGW breaking as a weak perturbation grows to nonlinear amplitudes, we perform direct numerical simulation using Dedalus[28] a spectral numerical method. Our region of interest is strictly interior to the WD and so our simulation must strive to eliminate boundary effects resulting from nonphysical boundaries. To do so, we adopt periodic boundary conditions in the x direction and damping layers (described in §IV B) in the z direction to damp perturbations exiting the domain. Correspondingly, we use a Fourier basis in the x direction and a Chebyshev in the z direction.

A. Numerical Parameters

We nondimensionalize by taking $H = N = \rho_0(z = 0) = 1$ in Eq. 1.

Our simulation starts with all perturbation quantities at zero. We choose as follows:

- k_{0x}: Astrophysical IGWs have $k_{0x} \ll k_{0z}$, so we choose $k_{0x} = \frac{2\pi}{L_x}$ the smallest permitted wavenumber permitted by periodic boundary conditions.
- We choose ω_0 by choosing it to produce a desired k_{0z}. Astrophysical systems generally also exhibit $k_{0z}H \gg 1$, where the stratification height is significantly larger than the vertical wavelength. However, in order for the simulation to both be well-damped at grid resolutions and be neglibily damped at leading order nonlinear wavelengths, we require $k_{0z} \ll \frac{1}{L_{NL}} \ll \frac{2\pi N_z}{L_z}$, where L_{NL} denotes some characteristic length scale of nonlinear features. Finally, we need L_z to be many H to capture significant $e^{z/2H}$ growth and separate the linear and nonlinear amplitudes of u_z.

  Fixing $L_z = 10H$ to give $\sim e^4$ amplitude growth between the damping zones, this implies we require

[2] In practice, σ must be large enough to be numerically resolved by the spectral code.

separation of scales $1 \ll k_{0z}H \ll \frac{H}{L_{NL}} \ll \frac{2\pi N_z}{10}$.

Since N_z is fixed by computational cost (we tried both $N_z = 512, N_z = 1024$), we choose $k_{0z} \sim \frac{2\pi}{H}$. This is less physically representative but gives more wavenumber space for the nonlinear cascade. We then invert $\omega_0 = \omega(k_{0x}, k_{0z})$.

- We choose F forcing strength 1/20 that of the nonlinear simulation, which keeps the flow amplitude sufficiently small to be treated in the linear approximation at all points in the simulation domain.

B. Damping Layers

To imitate an infinite fluid using a finite simulation domain, we use periodic boundary conditions in the x direction and damping layers at the top and bottom of the z direction. This damps waves that reach the edge of the simulation domain without inducing nonphysical reflection. Specifically, these are implemented by introducing linear damping terms to Eq. 2:

$$\begin{aligned} \frac{\mathrm{D}\Upsilon}{\mathrm{D}t} + u_z \frac{\partial \ln \rho_0}{\partial z} &= -\Gamma(z)\Upsilon, \\ \frac{\mathrm{D}\vec{u}}{\mathrm{D}t} + \vec{\nabla}P + P\vec{\nabla}\Upsilon + g\hat{z} &= -\Gamma(z)\vec{u}, \\ \frac{1}{2\tau}\left[2 + \tanh\frac{z - z_T}{\Delta z} + \tanh\frac{z_B - z}{\Delta z}\right] &= \Gamma(z), \end{aligned} \tag{12}$$

where $z_B = 0.05L_z, z_T = 0.95L_z$ are the boundaries of the damping zone. This strongly damps perturbations below z_B and above z_T with damping time τ, negligibly affects dynamics between z_B, z_T and has transition width governed by Δz; we use $\Delta z = 0.025L_z$. This prescription, used in similar studies[29], has the advantage of being smooth, important for spectral methods. As these damping terms are linear, they are retained in the linearized equations of motion as well.

The full implementation of the fluid equations in Dedalus is described in §A.

C. Linear Regime

We first test our numerical simulation with a "linear" simulation, where all flow quantities are small: we assume $\rho_1 \equiv \rho - \rho_0 \ll \rho_0$ and $\vec{u}\cdot\vec{\nabla} \ll \partial_t$. We emphasize that our "linear" simulations solve the full nonlinear equations, just in the weak perturbation limit.

ω is chosen by inverting $\omega(k_{0x}, k_{0z})$ dispersion relation for fixed $k_{0x} = 2\pi/L_x$ and some desired $k_{0z} = -2\pi/H$, and $\sigma \lesssim \frac{1}{k_{0z}}$ is used to excite a broad band of k_z modes including the desired k_{0z} mode.

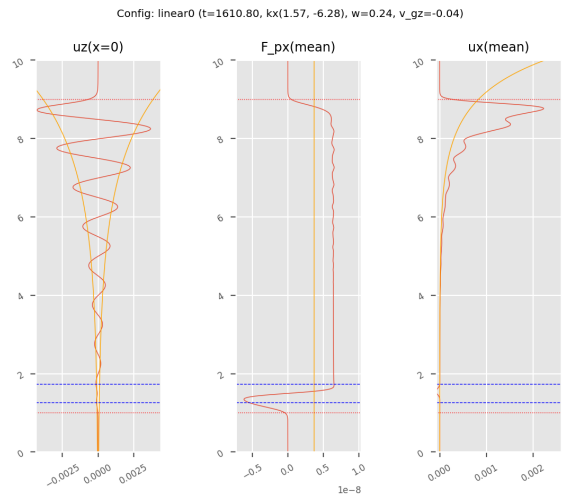

FIG. 1: Snapshot of linear simulation after reaching steady state. Analytical predictions of $|u_z|, \bar{U}_0, S_{px}$ are shown in orange. Red dotted lines indicate the onset of the damping region and blue dotted lines denote the driving region.

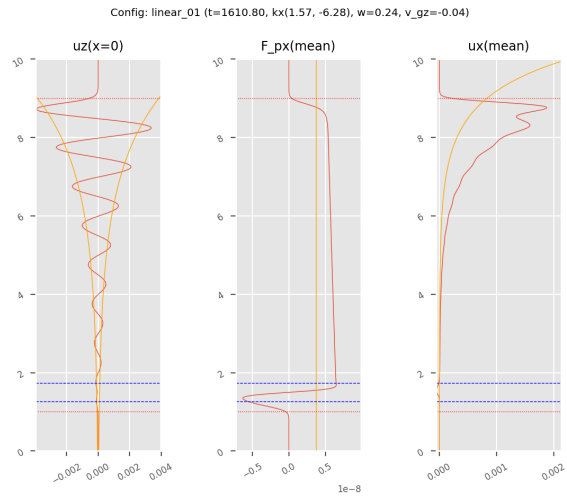

FIG. 2: Same as Fig. 1 but with 0.3×viscosity used for nonlinear simulations (YUBONOTE should be the same but that simulation mysteriously stopped without me noticing; restarting worked, so currently rerunning). Note the slight resulting dissipation in S_{px}.

D. Numerical Simulation

A representative snapshot of this simulation is provided in Fig. 1. Key features to note:

- u_z grows with Eq. 10 to reasonable accuracy.
- S_{px} is seen to be constant, as would be expected by Eq. 8.

We also include a qualitatively similar snapshot of the same simulation run using the ν from the later nonlinear simulations in Fig. 2.

E. Mean Flow Critical Layer Absorption

A Navier-Stokes numerical viscosity ν is used to damp high wavenumbers and regularize the nonlinear cascade at near grid resolution: $\nu \sim 0.2\frac{\omega}{|k_{0z}|}\frac{L_z}{2\pi N_z}$ was found to be suitable for $N_z = 1024$, where k_{0z} is the wavenumber of the excited linear mode.

In past studies of IGWs in WDs (cite Fuller & Lai), $\xi_z \equiv \frac{u_z}{\omega_0}$ the Lagrangian fluid displacement was often used towards wave breaking criterion $k_{0z}\xi_z \gtrsim 1$. We argue that the wave's self-interaction via its generated mean flow $\bar{U}_0$ induces total absorption when the mean flow exceeds critical value

$$\bar{U}_c = \frac{\omega_0}{k_{0x}}. \tag{13}$$

This is consistent with the picture put forth in e.g. Goldreich and Nicholson (cite).

A purely horizontal shear flow $\bar{U}_0(z)\hat{x}$ can be seen in Eq. 1 to have the effect of modifying time derivatives ∂_t to their frequency in the comoving frame of the fluid $\partial_t - \bar{U}_0(z)\partial_x$. For a critical value $\omega_0 - \bar{U}_c k_{0x} = 0$, the frequency of the linear wave in the fluid's frame of reference vanishes and critical behavior is observed. In a linear theory or a theory where small scales are viscosity rather than advection dominated, the incident wave has amplitude reflection and transmission coefficients

$$\mathcal{R} = e^{-2\pi\sqrt{\mathrm{Ri}-\frac{1}{4}}}, \qquad \mathcal{T} = e^{-\pi\sqrt{\mathrm{Ri}-\frac{1}{4}}}, \tag{14}$$

where we have defined Richardson number $\mathrm{Ri} \equiv \left.\frac{N^2}{\left(\frac{\partial \bar{U}_0}{\partial z}\right)^2}\right|_{z_c}$ at the critical layer $z_c : \bar{U}_0(z_c) = \frac{\omega_0}{k_{0x}}$. For most shear flows, $\mathrm{Ri} \gg 1$ and so $\mathcal{R}, \mathcal{T} \ll 1$ and the incident wave is absorbed.

When the fluid absorbs the incident wave, it absorbs the incident horizontal momentum flux as well, which is converted into additional horizontal momentum of the shear flow. Since the shear flow cannot exceed $\bar{U}_c$ the horizontal phase velocity of the incident wave, the critical layer must thus propagate downwards (towards the wave source) to accommodate the incident momentum. In other words, the total horizontal momentum of the shear flow obeys conservation equation

$$\frac{\partial}{\partial t}\int_0^{L_z} \rho(z)\bar{U}_0(z,t)\,\mathrm{d}z - S_{px} = 0. \tag{15}$$

Treating $\bar{U}_0(z > z_c) = \bar{U}_c, \bar{U}(z < z_c) = 0$ gives us exactly

$$\rho\bar{U}_c\frac{\partial z_c}{\partial t} = -S_{px}. \tag{16}$$

For constant S_{px} in space and $\rho \approx \rho_0$, this has analytical solution

$$z(t) = -H\ln t - H\ln\frac{H\rho_0(z=0)c_{ph,x}}{S_{px}}. \tag{17}$$

F. Numerical Simulation

We use the same k_{0x}, ω_0 as §IV D. Our other parameters are:

- We choose $\nu = 0.35\frac{\omega_0}{k_{0z}k_{z,\max}}$, where $k_{z,\max} = \frac{2\pi N_z}{L_z}$. Note that $\nu = \frac{\omega_0}{k_{0z}k_{z,\max}}$ corresponds to the advective term $\vec{u}\cdot\vec{\nabla}$ being of the same order as the time derivative ∂_t for flow velocities $\vec{u} \sim \frac{\omega_0}{k_{0z}}$ at the grid spacing.

Two representative snapshots from our simulation are provided in Fig. 3 after the critical layer has had time to form. We may note that the critical layer, where S_{px} is absorbed and $\bar{U}_0 = \bar{U}_c$, travels downwards as predicted.

G. Propagating Critical Layer

For the simulation in Fig. 3, we may define $z_c = \mathrm{argmax}_z \frac{\partial \bar{U}_0}{\partial z}$. Computing $\frac{\partial z_c}{\partial t}$ using the analytical flux Eq. 8 allows comparison to Eq. 16, which we exhibit in Fig. 4. We see overall good agreement, though some small deviation is expected since S_{px} is not perfectly conserved owing to numerical viscosity (and YUBONOTE S_{px} is misestimated?).

However, recalling Eq. 14, we only expect complete critical layer absorption when $\mathrm{Ri} \gg \frac{1}{4}$. We may plot Ri over the same time interval in Fig. 5. We may observe that the Richardson number is initially decreasing but eventually levels out and begins to increase again. This corresponds to an increasingly sharp critical layer transition then subsequently a decreasingly sharp critical layer transition.

We argue that the Richardson number is bounded from below by viscosity. A repeated simulation with a larger viscosity is shown in Fig. 6, where the Richardson number does not go nearly as low.

V. DISCUSSION

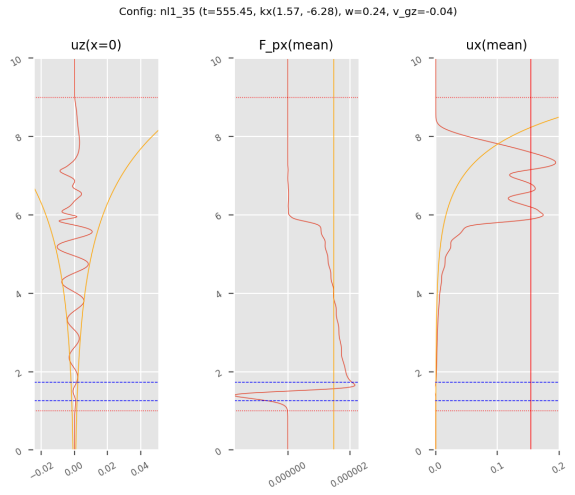

(a) Earlier time snapshot. Legend is the same as Fig. 1 except $\bar{U}_c$ is marked in red on the third panel.

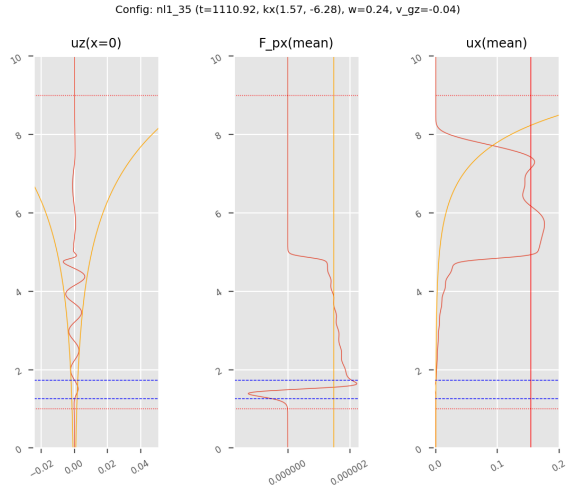

(b) Later snapshot illustrating propagation of z_c.

FIG. 3: Nonlinear numerical simulation.

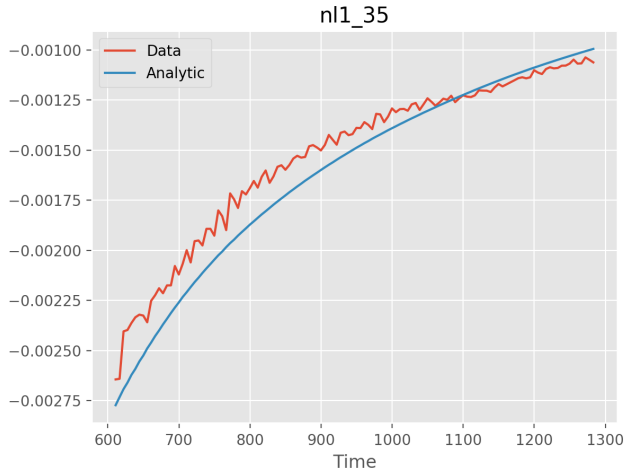

FIG. 4: Comparison of simulated $\frac{\partial z_c}{\partial t}$ to analytical Eq. 16. Plot begins after formation of critical layer in simulation.

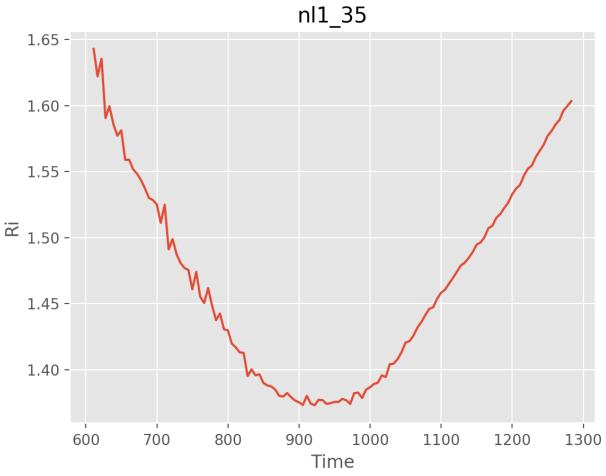

FIG. 5: Plot of $\mathrm{Ri}_{\max}(t) = \max_z \frac{N^2}{U_0'}(t)$ over the simulation time.

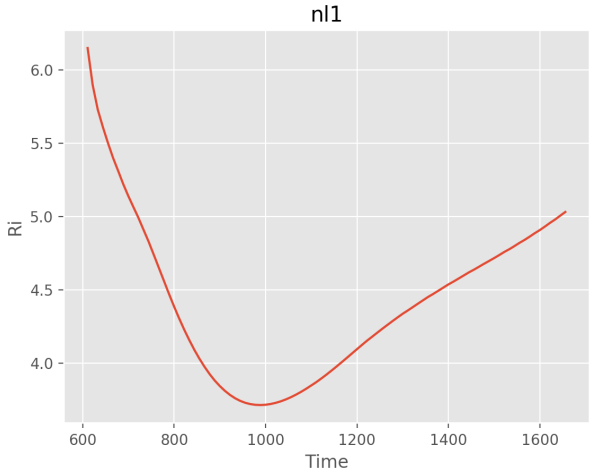

FIG. 6: Same as Fig. 5 but with $\sim 1.3\times$ viscosity.

Appendix A: Equation Implementations

We denote $x \in [0, L_x], z \in [0, L_z]$ the simulation domain and N_x, N_z the number of spectral modes in the respective dimensions. We perform direct numerical simulation of Eq. 9 with the open-source pseudo-spectral code Dedalus (CITE).

Numerically, the nonlinear $\frac{\vec{\nabla} P}{\rho}$ term is problematic: we desire a system where the fluid fields are not divided by one another. We introduce $\varpi = \frac{P}{\rho}$ instead, then mandate ρ_0, ϖ_0 background fields satisfy hydrostatic equilibrium $\vec{\nabla}\varpi_0 + \varpi_0\vec{\nabla}\rho_0 + g\hat{z} = 0$. Taking isothermal stratification, we find $\varpi_0 = gH$. We further change variables to $\Upsilon = \ln\rho - \ln\rho_0$ and $\varpi_1 = \varpi - \varpi_0$ deviations from the background state to obtain a system of equations at most quadratic in fluid fields:

$$\vec{\nabla}\cdot\vec{u} = 0, \tag{A1a}$$

$$\frac{\partial\Upsilon}{\partial t} + \Big(\vec{u}\cdot\vec{\nabla}\Big)\Upsilon - \frac{u_z}{H} = 0, \tag{A1b}$$

$$\frac{\partial u_x}{\partial t} + \Big(\vec{u}\cdot\vec{\nabla}\Big)u_x + \frac{\partial\varpi_1}{\partial x} + gH\frac{\partial\Upsilon}{\partial x} + \varpi_1\frac{\partial\Upsilon}{\partial x} = 0, \tag{A1c}$$

$$\frac{\partial u_z}{\partial t} + \Big(\vec{u}\cdot\vec{\nabla}\Big)u_z + \frac{\partial\varpi_1}{\partial z} + gH\frac{\partial\Upsilon}{\partial z} + \varpi_1\frac{\partial\Upsilon}{\partial z} - \frac{\varpi_1}{H} = 0. \tag{A1d}$$

It bears noting that these equations are exactly equivalent to the original Euler equations and hence conserve horizontal momentum.

1. Artificial Dissipation

The nonlinear terms in the above equations will transfer energy from lower wavenumbers to higher wavenumbers. Since spectral codes have no numerical dissipation, artificial dissipation must be added. To ensure the dissipitive system conserves horizontal momentum, we begin by adding dissipitive terms to the flux-conservative form of the Euler fluid equations Eq. 1 (we use stress tensor $\tau_{ij} = P\delta_{ij}$):

$$\vec{\nabla}\cdot\vec{u} = 0, \tag{A2a}$$

$$\partial_t\rho + \vec{\nabla}\cdot(\rho\vec{u} - \nu\vec{\nabla}(\rho - \rho_0)) = 0, \tag{A2b}$$

$$\partial_t(\rho\vec{u}) + \vec{\nabla}\cdot(\rho\vec{u}\vec{u} + \mathrm{diag}(\rho\varpi) - \nu\rho\vec{\nabla}\vec{u}) + \rho g\hat{z} = 0. \tag{A2c}$$

The same ν is used for both the diffusive and viscous term, though this is not required. Since the dissipation is not physical and is purely used for numerical stability, we choose it such that hydrostatic equilibrium is not modified. Some algebraic manipulation to re-cast it in the form of Eq. A1 gives

$$\vec{\nabla}\cdot\vec{u} = 0, \tag{A3a}$$

$$\partial_t\Upsilon + \Big(\vec{u}\cdot\vec{\nabla}\Big)\Upsilon - \frac{u_z}{H} - \nu\bigg(\nabla^2\Upsilon + \Big(\vec{\nabla}\Upsilon\Big)\cdot\Big(\vec{\nabla}\Upsilon\Big) - \frac{2}{H}\partial_z\Upsilon + \frac{1-e^{-\Upsilon}}{H^2}\bigg) = 0, \tag{A3b}$$

$$\begin{aligned}\partial_t\vec{u} + \Big(\vec{u}\cdot\vec{\nabla}\Big)\vec{u} + \vec{\nabla}\varpi + \varpi\vec{\nabla}\Upsilon - \nu\nabla^2\vec{u} + \vec{u}\nu\bigg(\nabla^2\Upsilon + \Big(\vec{\nabla}\Upsilon\Big)\cdot\Big(\vec{\nabla}\Upsilon\Big) - \frac{2}{H}\partial_z\Upsilon + \frac{1-e^{-\Upsilon}}{H^2}\bigg)& \\ -2\nu\bigg(\Big(\Big(\vec{\nabla}\Upsilon\Big)\cdot\vec{\nabla}\Big)\vec{u} - \frac{1}{H}\partial_z\vec{u}\bigg) - \frac{\varpi_1}{H} = 0.&\end{aligned} \tag{A3c}$$

Hydrostatic equilibrium is still $\vec{\nabla}\varpi_0 + g\hat{z} = 0$ where $\rho = \rho_0, \vec{u} = 0$. Including the damping layers and forcing terms as described in §IV A, we finally obtain the full system of equations as simulated in Dedalus:

$$\vec{\nabla}\cdot\vec{u} = 0, \tag{A4a}$$

$$\begin{aligned}\partial_t\Upsilon - \frac{u_z}{H} = \nu\bigg(\nabla^2\Upsilon + \Big(\vec{\nabla}\Upsilon\Big)\cdot\Big(\vec{\nabla}\Upsilon\Big) - \frac{2}{H}\partial_z\Upsilon + \frac{1-e^{-\Upsilon}}{H^2}\bigg),\\ - \Big(\vec{u}\cdot\vec{\nabla}\Big)\Upsilon - \Gamma(z)\Upsilon + \frac{F}{\rho_0(z)}e^{-\frac{(z-z_0)^2}{2\sigma^2}}\cos(k_x x - \omega t),\end{aligned} \tag{A4b}$$

$$\begin{aligned}\frac{\partial u_x}{\partial t} + \frac{\partial T}{\partial x} + gH\frac{\partial\Upsilon}{\partial x} = \nu\nabla^2 u_x - u_x\nu\bigg(\nabla^2\Upsilon + \Big(\vec{\nabla}\Upsilon\Big)\cdot\Big(\vec{\nabla}\Upsilon\Big) - \frac{2}{H}\partial_z\Upsilon + \frac{1-e^{-\Upsilon}}{H^2}\bigg)\\ + 2\nu\bigg(\Big(\Big(\vec{\nabla}\Upsilon\Big)\cdot\vec{\nabla}\Big)u_x - \frac{1}{H}\partial_z u_x\bigg) - \Gamma(z)u_x - \Big(\vec{u}\cdot\vec{\nabla}\Big)u_x - T_1\frac{\partial\Upsilon}{\partial x},\end{aligned} \tag{A4c}$$

$$\begin{aligned}\frac{\partial u_z}{\partial t} + \frac{\partial T}{\partial z} + gH\frac{\partial\Upsilon}{\partial z} - \frac{T_1}{H} = \nu\nabla^2 u_z - u_z\nu\bigg(\nabla^2\Upsilon + \Big(\vec{\nabla}\Upsilon\Big)\cdot\Big(\vec{\nabla}\Upsilon\Big) - \frac{2}{H}\partial_z\Upsilon + \frac{1-e^{-\Upsilon}}{H^2}\bigg)\\ + 2\nu\bigg(\Big(\Big(\vec{\nabla}\Upsilon\Big)\cdot\vec{\nabla}\Big)u_z - \frac{1}{H}\partial_z u_z\bigg) - \Gamma(z)u_z - \Big(\vec{u}\cdot\vec{\nabla}\Big)u_z - T_1\frac{\partial\Upsilon}{\partial z}.\end{aligned} \tag{A4d}$$

[1] G. Nelemans, Class. Quantum Grav **26**, 094030 (2009).
[2] H. B. Perets, A. Gal-Yam, P. Mazzali, D. Arnett, D. Kagan, A. V. Filippenko, W. Li, I. Arcavi, S. B. Cenko, D. Fox, *et al.*, Nature **465**, 322 (2010).
[3] E. García-Berro, C. Badenes, G. Aznar-Siguán, and P. Lorén-Aguilar, MNRAS **468**, 4815 (2017).
[4] J. Fuller and D. Lai, ApJL **756**, L17 (2012).
[5] I. Iben Jr and A. V. Tutukov, ApJS **54**, 335 (1984).
[6] R. Webbink, ApJ **277**, 355 (1984).
[7] M. Gilfanov and Á. Bogdán, Nature **463**, 924 (2010).
[8] D. Maoz, K. Sharon, and A. Gal-Yam, ApJ **722**, 1879 (2010).
[9] V. Korol, E. M. Rossi, P. J. Groot, G. Nelemans, S. Toonen, and A. G. A. Brown, MNRAS **470**, 1894 (2017).
[10] K. J. Shen, D. Boubert, B. T. Gänsicke, S. W. Jha, J. E. Andrews, L. Chomiuk, R. J. Foley, M. Fraser, M. Gromadzki, J. Guillochon, M. M. Kotze, K. Maguire, M. R. Siebert, N. Smith, J. Strader, C. Badenes, W. E. Kerzendorf, D. Koester, M. Kromer, B. Miles, R. Pakmor, J. Schwab, O. Toloza, S. Toonen, D. M. Townsley, and B. J. Williams, AJ **865**, 15 (2018).
[11] M. Kilic, N. C. Hambly, P. Bergeron, C. Genest-Beaulieu, and N. Rowell, MNRAS **479**, L113 (2018).
[12] J. Fuller and D. Lai, MNRAS **421**, 426 (2012).
[13] J. Fuller and D. Lai, MNRAS **412**, 1331 (2011).
[14] J. Fuller and D. Lai, MNRAS **430**, 274 (2013).
[15] K. B. Winters and E. A. D'Asaro, J. Fluid Mech **272**, 255–284 (1994).
[16] A. J. Barker and G. I. Ogilvie, MNRAS **404**, 1849 (2010).
[17] P. Drazin, Proc. R. Soc. Lond. A **356**, 411 (1977).
[18] H. Dosser and B. Sutherland, Physica D: Nonlinear Phenomena **240**, 346 (2011).
[19] H. V. Dosser and B. R. Sutherland, J. Atmos. Chem. **68**, 2844 (2011).
[20] J.-P. Zahn, A&A **41**, 329 (1975).
[21] P. Goldreich and P. D. Nicholson, ApJ **342**, 1079 (1989).
[22] R. S. Lindzen and J. R. Holton, Journal of the Atmospheric Sciences **25**, 1095 (1968), https://doi.org/10.1175/1520-0469(1968)025¡1095:ATOTQB¿2.0.CO;2.
[23] J. Klostermeyer, Geophysical & Astrophysical Fluid Dynamics **61**, 1 (1991), https://doi.org/10.1080/03091929108229035.
[24] J. R. Booker and F. P. Bretherton, J. Fluid Mech **27**, 513–539 (1967).
[25] P. Hazel, J. Fluid Mech **30**, 775–783 (1967).
[26] S. Brown and K. Stewartson, Journal of Fluid Mechanics **115**, 217 (1982).
[27] D. Andrews and M. E. Mcintyre, Journal of the Atmospheric Sciences **33**, 2031 (1976).
[28] K. J. Burns, G. M. Vasil, J. S. Oishi, D. Lecoanet, and B. Brown, "Dedalus: Flexible framework for spectrally solving differential equations," Astrophysics Source Code Library (2016), ascl:1603.015.
[29] D. Lecoanet, G. M. Vasil, J. Fuller, M. Cantiello, and K. J. Burns, Monthly Notices of the Royal Astronomical Society **466**, 2181 (2016), http://oup.prod.sis.lan/mnras/article-pdf/466/2/2181/10868477/stw3273.pdf.